

FULL PAPER

Molecular and electronic properties of Schiff bases derived from different aniline derivatives: density functional theory study

Ali J. A. Al-Sarray* 

Department of Chemistry, College of Science,
University of Baghdad, Baghdad, Iraq

Herein, five Schiff base molecules derived from para-nitrobenzaldehyde and different aniline derivatives are studied theoretically from the structure and energy perspectives. Density functional theory DFT method with 6-31+g(d,p) basis set is utilized to determine the optimized structure with the lowest energy in terms of the internal coordinates such as bond lengths, bond angles, and torsion angles. The study includes investigating the electronic indicators of the title molecules, such as frontier molecular orbital, electron affinity, ionization potential, and other parameters to predict the sites of reactivity and obtain an insight of the main properties of the molecules. Moreover, the electrostatic potential maps were determined and illustrated for the studied compounds to investigate the reactivity of charges on the surface of the molecules whether being of an electrophilic or nucleophilic nature. The study aims to examine the effect of changing the functional group in para-location of the aniline moieties on the molecular and geometrical properties of the molecules.

*Corresponding Author:

Ali J.A. Al-Sarray

Email: albaghdady1993@gmail.com,

ali.j@sc.uobaghdad.edu.iq

Tel.: +9647716343326

KEYWORDS

DFT; electrostatic potential; FMO; Schiff base; optimization; molecular structure.

Introduction

In the last couple of decades, Schiff base molecules attracted a considerable attention among researchers [1,2] due to the unique properties that they exhibit which favor them for a wide range of applications in the field of medicinal and catalysis chemistry [3]. Some of the features that make Schiff bases very special species are being anti-toxic, anti-inflammatory, anti-cancer, and anti-bacterial agents [4]. This class of organic molecules are containing a distinctive functional group which formed by carbon and nitrogen atoms linked via double bond. Schiff bases are prepared from reacting an aldehyde or a ketone with a primary amine molecule. Many studies have concluded that using aromatic

compounds that contain carbonyl group will contribute to the high stability of produced Schiff bases compared to aliphatic moieties that increase the polymerization ability. Moreover, aromatic Schiff bases are found to be relatively safer when used as therapeutic agents [5]. In terms of geometrical aspect of the aromatic Schiff bases, some researchers suggest that most of the thermochromic Schiff base molecules are planar, whereas the others that are non-planar are exhibiting photochromism [6,7]. On the other hand, determining the stability of Schiff base structures using theoretical calculations and drug design modeling is considered as a high priority to expand our understanding of this kind of organic species [8]. These computational methods can predict various

molecular properties, including electrostatic potentials, vibrational frequencies, non-linear optical merits [9,10]. One of the famous methods that suit these kinds of calculations is density functional theory DFT which represent a post-HF approach that enables the researchers to predict the molecular energies [11], the characteristics of structures [12], and spectroscopic properties with high accuracy [13]. Koopmans' theorem and total energy calculations are performed in this study for the titled molecules, including these that are connected with frontier molecular orbitals. Some other quantities are evaluated in the framework molecular orbitals providing a valuable insight when it comes to the molecular properties of the studied compounds.

Materials and methods

The computational calculations performed in this study are according to the density functional theory method using hybrid functional of three parameters (the Becke) and correlation functional of (LYP) which represents one the hybrid family with the most robust functional. The Basis set that is used for herein calculation was 6-31+g(d,p) which is very suitable for this kind of molecules as reported by many researchers. The studied molecules listed in (Table 1) were prepared and characterized

previously [14,15]. Koopmans' theorem was applied to carry out the electronic properties of the Schiff base and obtain the frontier molecular orbitals [16]. The electron affinity (EA) and ionization potential (IP) were calculated depending on the HOMO-LUMO values. The other parameters were obtained according to these values, including softness (r), hardness (χ), electrochemical potential (μ), electronegativity (η), and energy gap (ΔE) as stated in Equations 1-4 [17].

$$\mu = -\frac{1}{2}(I_P + E_A) \quad (1)$$

$$\eta = -\frac{1}{2}(E_{\text{HOMO}} + E_{\text{LUMO}}) \quad (2)$$

$$\chi = -\frac{1}{2}(E_{\text{HOMO}} - E_{\text{LUMO}}) \quad (3)$$

$$\Delta E = (E_{\text{LUMO}} - E_{\text{HOMO}}) \quad (4)$$

Reactivity parameters were also determined, including net electrophilicity (ω^\pm), electronic donating power (ω^-), electronic withdrawing power (ω^+), and electrophilicity Index (ω) [18] according to the Equations 5-8 [19].

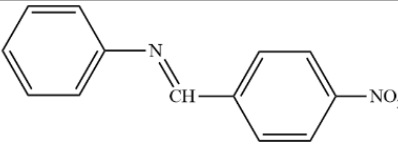
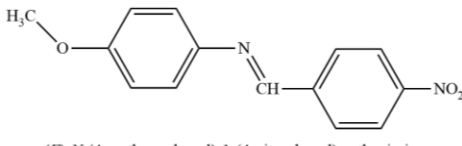
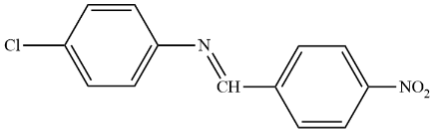
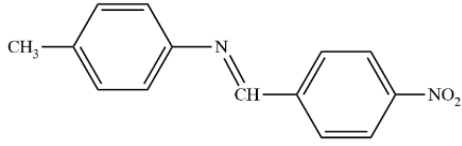
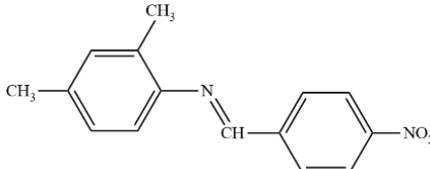
$$\omega = \frac{\mu^2}{2\chi} \quad (5)$$

$$\omega^- = \frac{(3I_P + 3E_A)^2}{16(I_P - E_A)} \quad (6)$$

$$\omega^+ = \frac{(I_P + 3E_A)^2}{16(I_P - E_A)} \quad (7)$$

$$\omega^\pm = \omega^+ - (-\omega^-) \quad (8)$$

TABLE 1 Chemical structures of the studied molecules and their abbreviations

Compound	Abbreviation
 <i>(E)</i> -1-(4-nitrophenyl)- <i>N</i> -phenylmethanimine	Ani-N
 <i>(E)</i> - <i>N</i> -(4-methoxyphenyl)-1-(4-nitrophenyl)methanimine	Pan-N
 <i>N</i> -(4-chlorophenyl)-1-(4-nitrophenyl)methanimine	Pcl-N
 1-(4-nitrophenyl)- <i>N</i> -(<i>p</i> -tolyl)methanimine	Pto-N
 <i>(E)</i> - <i>N</i> -(2,4-dimethylphenyl)-1-(4-nitrophenyl)methanimine	Xyl-N

Results and discussion

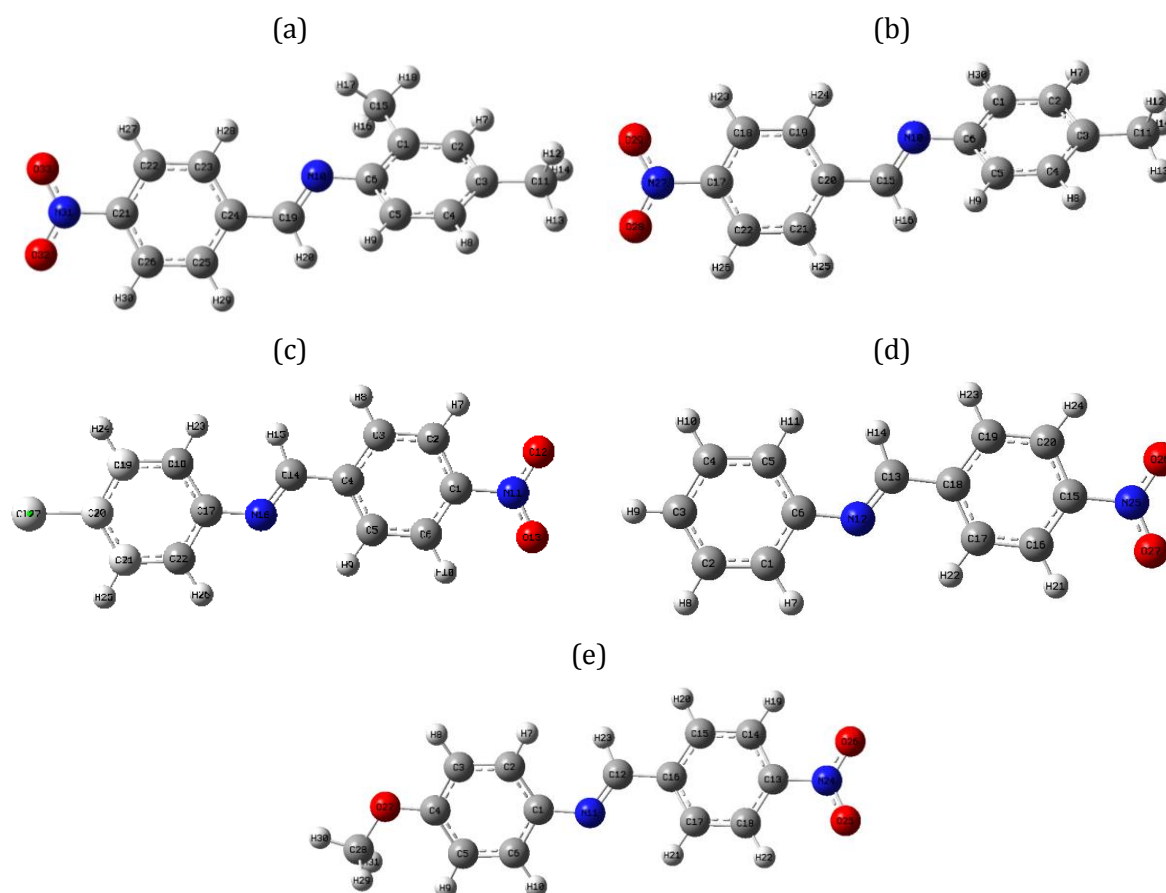
The structural geometries of the studied molecules were determined after optimization using B3LYP/6-31+g(d,p) basis set of DFT method in terms of bond lengths and angles as well as the dihedral angles as listed in Tables 4 to 8). The optimization parameters were obtained for the most stable geometries (Figure 1) after many optimizing steps which indicate that (Pan-N) compound has the least total energy with the following trend for stability:

$$Pcl-N < Ani-N < Pto-N < Xyl-N < Pan-N$$

The other parameters of optimization were included in Table 2. All the geometries of investigated compounds have a symmetry point group of C1 with stationary points that are related to the local minima structures on the PE surfaces. Figure 1 illustrates the optimized structures of the studies molecules with atoms numbering that is consistent with the tables of geometry parameters.

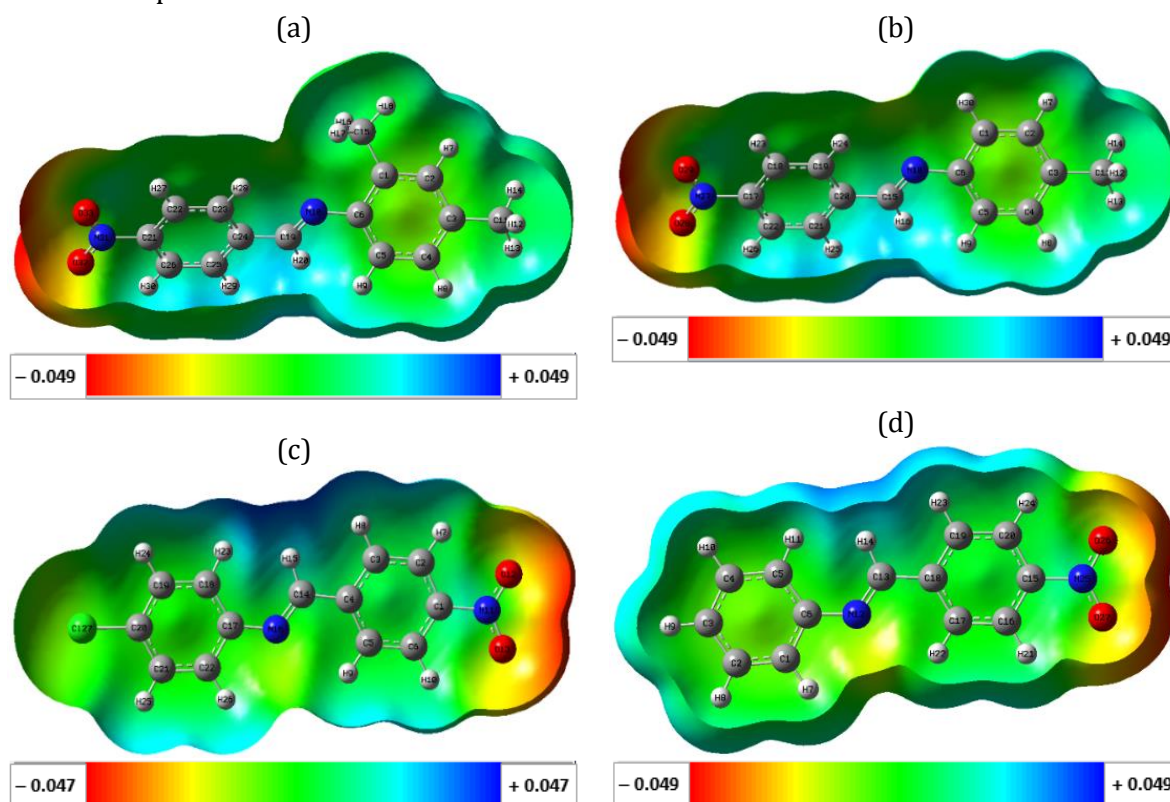
TABLE 2 The optimization parameters of the most stable structures of Schiff base compounds

Optimization Parameter	Xyl-N	Pto-N	Ani-N	Pcl-N	Pan-N
Total Energy (Hartree)	-875.828	-839.94	-800.62	-761.297	-1220.89
Dipole Moment (Debye)	6.0668	6.405	6.1334	4.2282	7.2183
RMS Gradient Norm (Hartree/Bohr)	0.000011	0.000001	0.000004	0.000025	0.000028
Max. Force (Hartrees/Bohr-Radians)	0.000037	0.000001	0.000013	0.000084	0.000087
RMS Force (Hartrees/Bohr-Radians)	0.000007	0.000000	0.000002	0.000016	0.000017
Max. Displacement (Bohr-Radians)	0.00119	0.0022	0.00178	0.00076	0.00078
RMS Displacement (Bohr-Radians)	0.00025	0.00033	0.0003	0.00023	0.00021

**FIGURE 1** The optimized structures with the lowest energy according to DFT-B3YLP/6-31+g(d,p) for the compound Xyl-N (a), Pto-N (b), Pcl-N (c), Ani-N (d), and Pan-N (e)

To obtain the details of the electrostatic effect at a certain point in the space that surround the molecule, the electrostatic potential maps are used to illustrate the correlation of the net charge distribution, including the nuclei and electron charges, with chemical reactivities, partial charges, electronegativities, and dipole moments. The ESP method provides an efficient data to visualize the relative polarities of the molecules under study [20]. The negative electrostatic potential illustrates the highly attractive properties of the condensed electron density to attract the proton, whereas the electrostatic potential that is positive illustrate the highly repulsive properties of low electron density regions, which represent the atomic nuclei charges that are shielded incompletely, toward the protons [21]. The electrostatic potentials were calculated for all

studied compounds using the same method used for optimization and their surfaces were illustrated in Figure 2 where the reactive sites as well as the densities, shapes, and sizes of the molecular charges are depicted [22]. Different colors are used to evaluate the values of electrostatic potentials, including blue color reflecting the electrostatic potential that is highly positive, red color reflects the highly negative electrostatic potential, and green color reflects the regions that are possessing zero potential [23]. All the surfaces of studied compounds showed a highly negative charge distribution around the nitro groups indicating the ability of reacting with electrophilic site, whereas the hydrogen atoms of the rings and the methyl groups showed poor charge densities indicating the high ability of reacting with nucleophilic site.



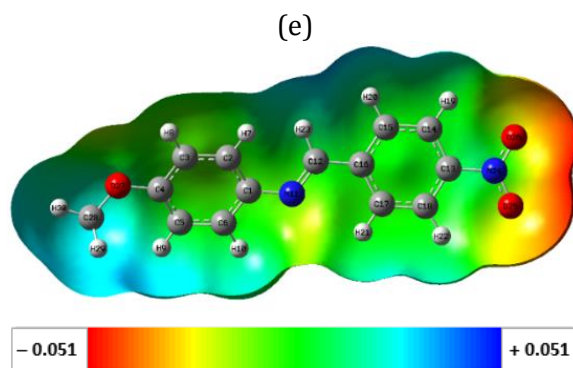


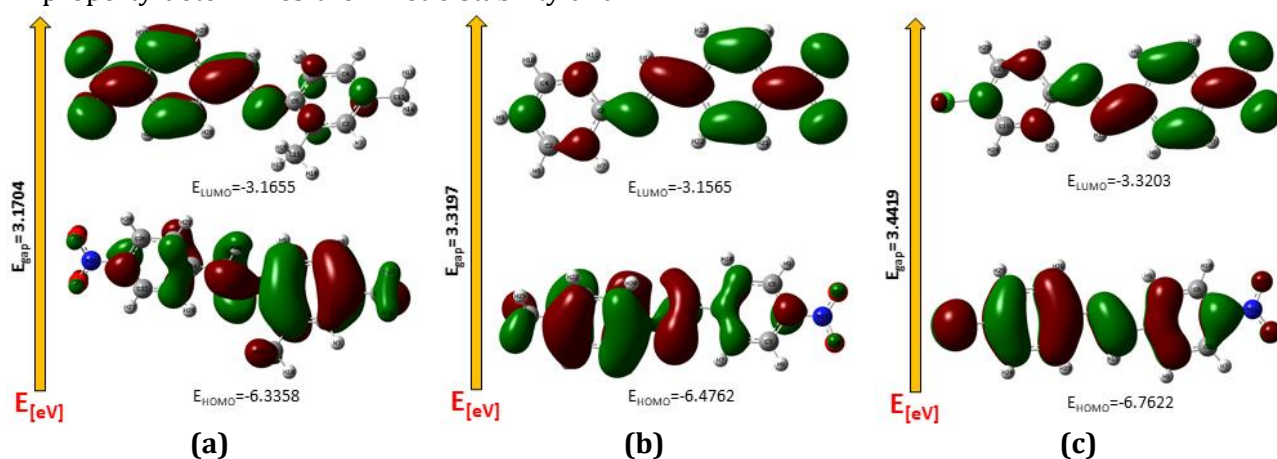
FIGURE 2 The electrostatic potential surfaces of the studied compound Xyl-N (a), Pto-N (b), Pcl-N (c), Ani-N (d), and Pan-N (e)

To determine the nature of interaction between the studied molecules and the other species, frontier molecular orbital study is the suitable for such calculations. The electrons that are located at the outermost orbitals tend to be donated which can be obtained by determining the highest occupied orbitals (HOMO). On the other hand, the free spaces of the innermost orbitals tend to accept electrons obtained by determining the lowest unoccupied orbitals (LUMO). The energy of HOMO and LUMO can be connected directly to the ionization potential and electron affinity, respectively. One of the important properties concluded from these energies is the energy gap which represents the difference in energy between HOMO and LUMO orbitals, and this property determines the kinetic stability and

chemical reactivity of the molecules [25]. Small values of energy gap indicate that the molecule is highly polarized, and therefore, being a soft molecule. Moreover, energy gap is commonly used as electron conductivity indicator to determine the molecules' bioactivity when inferred from the intra-molecule charge transfer (ICT). The studied molecules have shown relatively low energy gaps in the following trend:

$$Pan-N < Xyl-N < Pto-N < Pcl-N < Ani-N$$

The FMOs of the molecules under study are depicted in (Figure 3) and the energy values of HOMO, LUMO, and the other electronic parameters are listed in (Table 3).



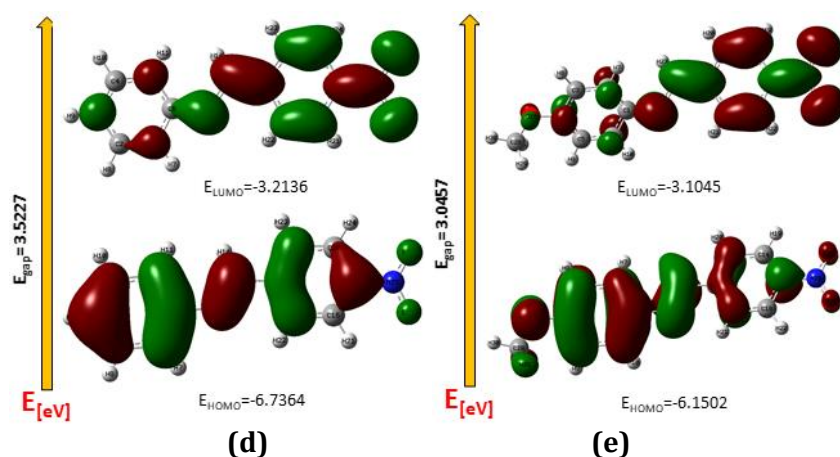


FIGURE 3 visualizing FMOs structures with the corresponding energies in eV for the compound Xyl-N (a), Pto-N (b), Pcl-N (c), Ani-N (d), and Pan-N (e)

TABLE 3 The energy values of the frontier molecular orbital parameters

Parameter	Xyl-N	Pto-N	Pcl-N	Ani-N	Pan-N
E_{HOMO}	-6.3358	-6.4762	-6.7622	-6.7364	-6.1502
E_{LUMO}	-3.1655	-3.1565	-3.3203	-3.2136	-3.1045
ΔE	3.1704	3.3197	3.4419	3.5227	3.0457
I_p	6.3358	6.4762	6.7622	6.7364	6.1502
EA	3.1655	3.1565	3.3203	3.2136	3.1045
μ	-4.7506	-4.8163	-5.0412	-4.9750	-4.6274
η	4.7506	4.8163	5.0412	4.9750	4.6274
χ	1.5852	1.6599	1.7210	1.7614	1.5229
ω	7.1186	6.9877	7.3837	7.0259	7.0303
ω^-	9.6921	9.6033	10.1195	9.7336	9.5344
ω^+	4.9414	4.7870	5.0782	4.7586	4.9070
ω_{\pm}	14.6335	14.3903	15.1977	14.4922	14.4414

* Energy values of HOMO (E_{HOMO}), LUMO (E_{LUMO}), Energy gap (ΔE), ionization potential (I_p), electron affinity (EA), chemical potential (μ), absolute electronegativity (η), absolute hardness (χ), electrophilicity index (ω), electron donating (ω^-), withdrawing (ω^+) powers, and net electrophilicity (ω_{\pm}).

TABLE 4 The bond lengths (Å), angles ($^\circ$), and torsional angles ($^\circ$) of (Xyl-N) compound

Bond lengths		Bond angles		Torsional angles	
C(01)-C(15)	1.5083	C(01)-C(02)-C(03)	122.745 $^\circ$	H(18)-C(15)-C(01)-C(02)	-11.3 $^\circ$
C(01)-C(02)	1.3981	C(01)-C(02)-H(07)	118.377 $^\circ$	C(02)-C(03)-C(11)-H(12)	+88.7 $^\circ$
C(02)-H(07)	1.0881	C(15)-C(01)-N(02)	120.946 $^\circ$	H(09)-C(05)-C(06)-N(10)	-0.53 $^\circ$
C(15)-H(17)	1.0944	C(01)-C(15)-H(16)	111.474 $^\circ$	C(06)-N(10)-C(19)-H(20)	-4.63 $^\circ$
C(06)-N(10)	1.4055	C(05)-C(06)-N(10)	122.475 $^\circ$	C(01)-C(06)-N(10)-C(19)	+145.4 $^\circ$
C(19)-N(10)	1.2812	C(06)-N(10)-C(19)	120.822 $^\circ$	H(20)-C(19)-C(24)-C(25)	-0.97 $^\circ$
C(19)-H(20)	1.0994	N(10)-C(19)-H(20)	121.925 $^\circ$	H(29)-C(25)-C(26)-H(30)	+0.04 $^\circ$
C(19)-C(24)	1.4704	C(24)-C(19)-H(20)	115.793 $^\circ$	H(30)-C(26)-C(21)-N(31)	+0.08 $^\circ$
C(21)-N(31)	1.4719	C(21)-N(31)-O(32)	117.789 $^\circ$	C(26)-C(21)-N(31)-O(32)	+0.04 $^\circ$
N(31)-O(32)	1.2329	O(32)-N(31)-O(33)	124.434 $^\circ$	C(22)-C(21)-N(31)-O(33)	+0.13 $^\circ$

TABLE 5 The bond lengths (Å), angles (°), and torsional angles (°) of (Pto-N) compound

Bond lengths		Bond angles		Torsional angles	
C(01)-C(02)	1.3923	C(01)-C(02)-C(03)	121.275°	C(06)-C(01)-C(02)-H(07)	+178.7°
C(02)-H(07)	1.0872	C(01)-C(02)-H(07)	119.271°	C(18)-C(17)-N(27)-O(28)	+179.9°
C(17)-N(27)	1.4720	C(18)-C(17)-N(27)	119.027°	C(21)-C(20)-C(15)-N(10)	+178.7°
N(27)-O(28)	1.2328	C(17)-N(27)-O(28)	117.786°	C(20)-C(15)-N(10)-C(06)	-177.3°
C(15)-C(20)	1.4702	O(28)-N(27)-O(29)	124.440°	H(16)-C(15)-N(10)-C(06)	-3.726°
C(15)-H(16)	1.0993	C(19)-C(20)-C(15)	121.523°	C(15)-N(10)-C(06)-C(05)	-33.97°
C(11)-N(13)	1.2745	C(20)-C(15)-H(16)	115.755°	N(10)-C(06)-C(01)-H(30)	-0.746°
N(10)-C(6)	1.4060	H(16)-C(15)-N(10)	122.127°	H(30)-C(01)-C(02)-C(03)	+179.1°
C(3)-C(11)	1.5104	C(15)-N(10)-C(06)	120.849°	C(02)-C(03)-C(11)-H(12)	-83.57°
C(11)-H(12)	1.0975	C(03)-C(11)-H(12)	111.083°	N(27)-C(17)-C(18)-H(23)	-0.008°

TABLE 6 The bond lengths (Å), angles (°), and torsional angles (°) of (Pcl-N) compound

Bond lengths		Bond angles		Torsional angles	
C(01)-C(02)	1.4059	C(01)-C(02)-C(03)	120.414°	C(01)-C(02)-C(03)-H(08)	+179.9°
C(02)-H(07)	1.0840	C(01)-C(02)-H(07)	118.781°	C(03)-C(04)-N(27)-O(29)	+177.8°
C(04)-N(27)	1.4796	C(03)-C(04)-N(27)	118.937°	C(06)-C(01)-C(11)-N(13)	+178.6°
N(27)-O(28)	1.2311	C(04)-N(27)-O(28)	117.724°	C(01)-C(11)-N(13)-C(14)	-178.8°
C(01)-C(11)	1.4649	O(28)-N(27)-O(29)	124.486°	H(12)-C(11)-N(13)-C(14)	-0.253°
C(11)-H(12)	1.1048	C(06)-C(01)-C(11)	119.174°	C(11)-N(13)-C(14)-C(16)	-48.01°
C(11)-N(13)	1.2745	C(01)-C(11)-H(12)	115.899°	N(13)-C(14)-C(16)-H(30)	-1.565°
N(13)-C(14)	1.4044	H(12)-C(11)-N(13)	123.404°	H(22)-C(19)-C(20)-C(23)	+0.779°
C(20)-C(23)	1.5095	C(11)-N(13)-C(14)	117.190°	C(19)-C(20)-C(23)-H(24)	-126.7°
C(23)-H(24)	1.0947	C(20)-C(23)-H(24)	111.455°	N(13)-C(14)-C(15)-H(18)	-0.065°

TABLE 7 The bond lengths (Å), angles (°), and torsional angles (°) of (Ani-N) compound

Bond lengths		Bond angles		Torsional angles	
C(01)-C(02)	1.3947	C(01)-C(02)-C(03)	120.006°	C(01)-C(02)-C(03)-H(09)	+180.0°
C(01)-H(07)	1.0852	C(01)-C(02)-H(08)	119.795°	C(02)-C(01)-C(06)-N(12)	-180.0°
C(06)-N(12)	1.4096	C(01)-C(06)-N(12)	115.442°	H(07)-C(01)-C(06)-N(12)	+0.000°
N(12)-C(13)	1.2815	C(06)-N(12)-C(13)	122.962°	C(01)-C(06)-N(12)-C(13)	-179.9°
C(13)-C(18)	1.4695	N(12)-C(13)-H(14)	123.303°	C(06)-N(12)-C(13)-H(14)	+0.000°
C(13)-H(14)	1.0983	H(14)-C(13)-C(18)	115.012°	N(12)-C(13)-C(18)-C(19)	+180.0°
C(15)-N(25)	1.4719	C(13)-C(18)-C(19)	119.239°	H(14)-C(13)-C(18)-C(19)	+0.000°
N(25)-O(26)	1.2330	C(20)-C(15)-N(25)	118.925°	H(24)-C(20)-C(15)-N(25)	+0.000°
		C(11)-N(13)-O(14)	124.426°	C(20)-C(25)-N(25)-O(27)	+180.0°

TABLE 8 The bond lengths (Å), angles (°), and torsional angles (°) of (Pan-N) compound

Bond lengths		Bond angles		Torsional angles	
C(01)-C(02)	1.4024	C(01)-C(02)-C(03)	120.738°	H(07)-C(02)-C(03)-H(08)	+1.055°
C(01)-N(11)	1.4036	C(01)-C(02)-H(07)	120.244°	H(08)-C(03)-C(04)-O(27)	+1.125°
C(12)-N(11)	1.2825	C(02)-C(01)-N(11)	124.672°	C(03)-C(04)-O(27)-C(28)	-179.0°
C(02)-H(07)	1.0856	C(01)-N(11)-C(12)	121.530°	C(04)-O(27)-C(28)-H(29)	+61.20°
C(04)-O(27)	1.3634	N(11)-C(12)-H(23)	122.409°	C(02)-C(01)-N(11)-C(12)	-26.84°
O(27)-C(28)	1.4239	H(23)-C(12)-C(16)	115.554°	C(01)-N(11)-C(12)-H(23)	-3.396°
C(28)-H(29)	1.0969	C(12)-C(16)-C(15)	119.258°	C(01)-N(11)-C(12)-C(16)	+177.7°
C(12)-H(23)	1.0990	C(14)-C(13)-N(24)	118.968°	H(20)-C(15)-C(16)-C(12)	-0.015°
C(12)-C(16)	1.4688	C(13)-N(24)-O(25)	117.799°	H(19)-C(14)-C(13)-N(24)	+0.047°
C(13)-N(24)	1.4708	O(25)-N(24)-O(26)	124.380	C(14)-C(13)-N(24)-O(25)	-179.9°
N(24)-O(25)	1.2329	C(04)-O(27)-C(28)	118.723		
		O(27)-C(28)-H(29)	111.295		

Conclusion

According to the computational calculations carried out based on B3LYP/6-31+g(d,p) basis set of the DFT method, the optimized structures of Schiff bases compounds are determined in terms of bond lengths, angles, and torsion angles. The FTOs study showed that the studied molecules exhibit small values of energy gaps which indicate the high bioactivity. The MEP maps illustrate that high electronic density in terms of negative potential located on the nitro groups of all studied compounds, whereas the regions of hydrogen atoms of the ring moieties exhibited positive potential. It can be concluded from the values of total energies of the most stable structures that the Pan-N compound possesses the highest stability with the least energy value.

Acknowledgements

The author would like to acknowledge the AJF for the assistance with sample acquisition and technical support.

Conflict of Interest

There is no conflict of interest.

Orcid:

Ali J.A. Al-Sarray:

<https://orcid.org/0000-0001-6484-1763>

References

- [1] B.K. Sarojini, P.S. Manjula, M. Kaur, B.J. Anderson, J.P. Jasinski, *Acta Crystallographica Section E: Structure Reports Online*, **2014**, *70*, o57-o58. [[Crossref](#)], [[Google Scholar](#)], [[Publisher](#)]
- [2] H. Tanak, F. Erşahin, Y. Köysal, E. Açar, Ş. Işık, M.Yavuz, *J. Mol. Model.*, **2009**, *15*, 1281-1290. [[Crossref](#)], [[Google Scholar](#)], [[Publisher](#)]
- [3] S. Kumar, V. Saini, I.K. Maurya, J. Sindhu, M. Kumari, R. Kataria, V. Kumar, *PLoS One*, **2018**, *13*, e0196016. [[Crossref](#)], [[Google Scholar](#)], [[Publisher](#)]
- [4] D.R. Williams, *Chem. Rev.*, **1972**, *72*, 203-213. [[Crossref](#)], [[Google Scholar](#)], [[Publisher](#)]
- [5] V.W. Barajas-Carrillo, A. Estolano-Cobián, L. Díaz-Rubio, R. Rosario Ayllón-Gutiérrez, R. Salazar-Aranda, Raúl Díaz-Molina, V. García-González, H. Almanza-Reyes, I.A. Rivero, Joaquín G. Marrero, I. Córdova-Guerrero, *Med. Chem. Res.*, **2021**, *30*, 610-623. [[Crossref](#)], [[Google Scholar](#)], [[Publisher](#)]
- [6] I. Moustakali-Mavridis, E. Hadjoudis, and A. Mavridis, *Acta Crystallographica Section B: Structural Crystallography and Crystal Chemistry*, **1978**, *34*, 3709-3715. [[Crossref](#)], [[Google Scholar](#)], [[Publisher](#)]
- [7] A.J. Al-Sarray, I.M. H. Al-Mousawi, and T. H. Al-Noor, *Chemical Methodologies*, **2022**, *6*, 331-338. [[Crossref](#)], [[Google Scholar](#)], [[Publisher](#)]
- [8] E. Hadjoudis, M. Vittorakis, I. Moustakali-Mavridis, *Tetrahedron*, **1987**, *43*, 1345-1360. [[Crossref](#)], [[Google Scholar](#)], [[Publisher](#)]
- [9] Y. Zhang, Z. Guo, X.-Z. You, *J. Am. Chem. Soc.*, **2001**, *123*, 9378-9387. [[Crossref](#)], [[Google Scholar](#)], [[Publisher](#)]
- [10] Y.B. Alpaslan, N. Süleymanoğlu, E. Öztekin, F. Erşahin, E. Açar, Ş. Işık, *J. Chem. Crystallogr.*, **2010**, *40*, 950-956. [[Crossref](#)], [[Google Scholar](#)], [[Publisher](#)]
- [11] C. Ravikumar, I.H. Joe, V. Jayakumar, *Chem. Phys. Lett.*, **2008**, *460*, 552-558. [[Crossref](#)], [[Google Scholar](#)], [[Publisher](#)]
- [12] R. Zhang, B. Du, G. Sun, Y. Sun, *Spectrochimica Acta Part A: Molecular and Biomolecular Spectroscopy*, **2010**, *75*, 1115-1124. [[Crossref](#)], [[Google Scholar](#)], [[Publisher](#)]
- [13] M. Kurt, T.R. Sertbakan, M. Ozduran, *Acta Part A: Mol. Biomol. Spectrosc.*, **2008**, *70*, 664-673. [[Crossref](#)], [[Google Scholar](#)], [[Publisher](#)]
- [14] A.J. Al-Sarray, I.M. Al-Mussawi, T.H. Al-Noor, Y. Abu-Zaid, *J. Med. Chem. Sci.*, **2022**, *5*, 1094-1101. [[Crossref](#)], [[Google Scholar](#)], [[Publisher](#)]

- [15] A.J.A. Al-Sarray, T. Al-Kayat, B.M. Mohammed, M.J.B. Al-assadi, Y. Abu-Zaid, *J. Med. Chem. Sci.*, **2022**, *5*, 1321-1330. [[Crossref](#)], [[Publisher](#)]
- [16] M. Ottonelli, M. Piccardo, D. Duce, S. Thea, G. Dellepiane, *Energy Procedia*, **2012**, *31*, 31-37. [[Crossref](#)], [[Google Scholar](#)], [[Publisher](#)]
- [17] D. Mamand, *Journal of Physical Chemistry and Functional Materials*, **2019**, *2*, 32-36. [[Pdf](#)], [[Google Scholar](#)], [[Publisher](#)]
- [18] R.G. Parr, L.v. Szentpály, S. Liu, *J. Am. Chem. Soc.*, **1999**, *121*, 1922-1924. [[Crossref](#)], [[Google Scholar](#)], [[Publisher](#)]
- [19] P.W. Ayers, *Faraday Discussions*, **2007**, *135*, 161-190. [[Crossref](#)], [[Google Scholar](#)], [[Publisher](#)]
- [20] F.J. Luque, M. Orozco, P.K. Bhadane, S.R. Gadre, *The Journal of Physical Chemistry*, **1993**, *97*, 9380-9384. [[Crossref](#)], [[Google Scholar](#)], [[Publisher](#)]
- [21] E.J. Brandas, J.R. Sabin, *Advances in quantum chemistry*. **2011**: Academic Press. [[Google Scholar](#)], [[Publisher](#)]
- [22] A. Sethi, R. Prakash, *Journal of Molecular Structure*, **2015**, *1083*, 72-81. [[Crossref](#)], [[Google Scholar](#)], [[Publisher](#)]
- [23] I. Alkorta, J.J. Perez, *International Journal of Quantum Chemistry*, **1996**, *57*, 123-135. [[Crossref](#)], [[Google Scholar](#)], [[Publisher](#)]

How to cite this article: Ali J.A. Al-Sarray*, Molecular and electronic properties of Schiff bases derived from different aniline derivatives: density functional theory study. *Journal of Medicinal and Pharmaceutical Chemistry Research*, 2023, 5(4), 317-326.